TECHNICAL NOTE

Radiation Medicine: Vol. 23 No. 5, 386–389 p.p., 2005

Ray Tracing Analysis of Overlapping Objects in Refraction Contrast Imaging

Masatsugu Hirano,[1] Katsuhito Yamasaki,[2] Hiroshi Okada,[3] Takashi Sakurai,[4] Takeshi Kondoh,[5] Tetsuro Katafuchi,[6] Kazuro Sugimura,[7] Sohei Kitazawa,[8] Riko Kitazawa,[8] Sakan Maeda,[8] and Shinichi Tamura[9]

We simulated refraction contrast imaging in overlapping objects using the ray tracing method. The easiest case, in which two columnar objects (blood vessels) with a density of 1.0 [g/cm^3], run at right angles in air, was calculated. For absorption, we performed simulation using the Snell law adapted to the object's boundary. A pair of bright and dark spot results from the interference of refracted X-rays where the blood vessels crossed. This has the possibility of increasing the visibility of the image.

Key words: synchrotron radiation, refraction contrast, ray tracing method, overlapping objects

Introduction

It is difficult to observe objects that have a small absorption difference using conventional absorption imaging, in spite of the rapid development of X-ray diagnostic devices. The practical application of a coherent X-ray source like laser is expected in the next generation. Refraction contrast imaging using highly coherent X-rays (synchrotron radiation) produces images that reflect objective density difference and have the possibility of clinical application. This imaging produces a bright/dark line pair at the object's boundary and has the effect of increasing visibility.[1-3] However, quantitative analysis of this imaging has not been carried out. Conventional sources have less coherence and are not able to produce such high-quality images. In this paper, refraction contrast imaging of crossing objects is simulated using the ray tracing method.[4] This paper assumes the existence of pillars with a density equal to water in air, for simplification of the X-ray imaging simulation.

Materials and Methods

The refraction index for X-rays is usually expressed as $n=1-\delta+i\beta$, where both δ and β are very small. δ is proportional to the density and square of the wavelength. For example, in water, δ is 2.3×10^{-7} and β is 1.2×10^{-10} at 30 keV. Therefore, the refraction index is much larger than the index of absorption. The real part of the refractive index is smaller than but close to 1.0. Therefore, the refraction angle is small. In Fig. 1, the refraction angle is 0.23 μrad (in the case of an incident angle of 45 degree).

Monte Carlo Simulation was applied to calculation of the travel paths of X-rays along the object surfaces, and absorption is considered in this paper. The number of photons radiated into the pixels of each detector was counted, and the number of counts was interpreted as intensity. Direction of X-ray at the margin of objects is calculated by the Snell law. This simulation program was originally developed by us. The program is described by C language.

The conditions were as follows in the calculation of ray tracing. The 30 keV monochromatic X-ray was exposed in air to the part at which two same-size pillars (diameter of 100 micrometers), assumed to be blood vessels with a density equal to 1.0 [g/cm^3], intersected at right angles (Fig. 2). The refraction contrast image

Received September 22, 2003; revision accepted September 25, 2004.

[1]Niihama National College of Technology

[2]Japan Synchrotron Radiation Research Institute

[3]Department of Urology, Teikyo University School of Medicine

Departments of [4]Internal and Geriatric Medicine, [5]Neurosurgery, [7]Radiology, and [8]Pathology, Kobe University Graduate School of Medicine

[6]National Cardiovascular Center

[9]Osaka University Graduate School of Medicine

Reprint requests to Masatsugu Hirano, Ph.D., Niihama National College of Technology, 7-1 Yagumo, Ehime 792-8580, JAPAN.

This work has been performed under the approval of the Photon Factory Program Advisory Committee (Proposal No. 2003P010).

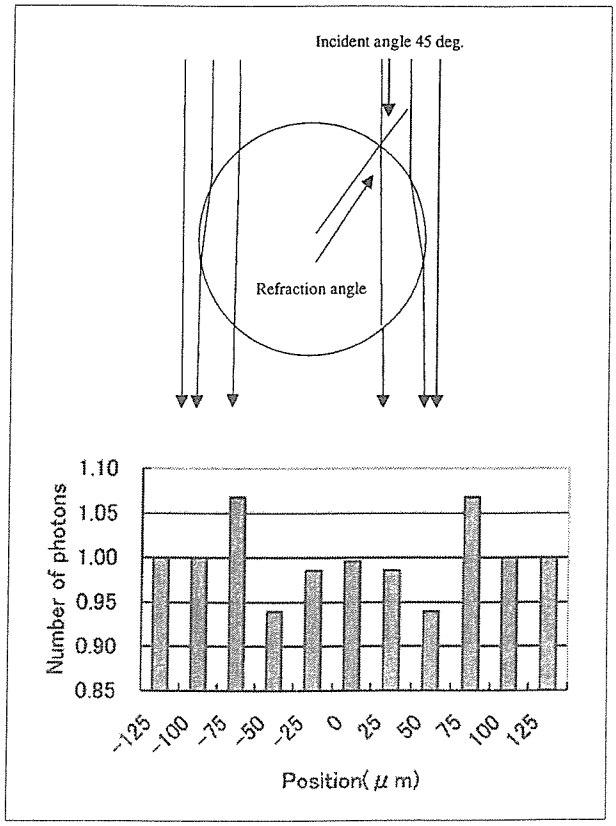

Fig. 1
A: Refraction contrast imaging. Parallel X-ray beams are bent by refraction, generating bright and dark lines outside and inside the boundary lines, respectively.
B: Profile curve of 30 keV X-ray refraction by pillars with a diameter of 100 μm (specific density = 1.0) observed with a detector in the case of a pixel size of 25 μm (the background is normalized to 1.0). Vertical numbers are photon counts into detector.

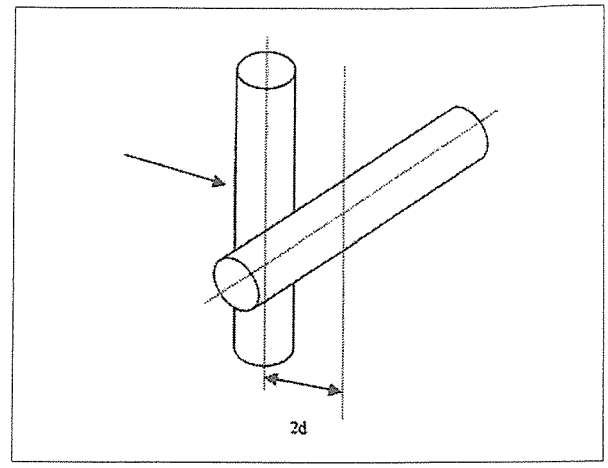

Fig. 2. Spatial relationship of two columns (diameter: d).

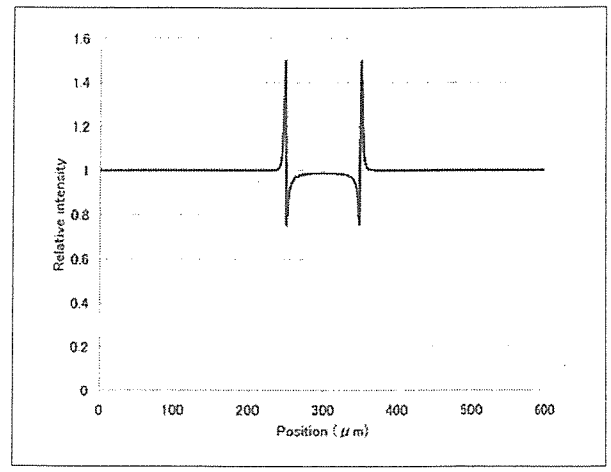

Fig. 3. Profile curve of the refraction image of a 100 μm cylinder.

was obtained 1[m] behind the sample. The ray tracing method was used in calculating parallel X-rays running at the surface of objects (Fig. 1). Finally, photons incident to each pixel (pixel size, 1 micrometer) of the detector were counted, and the number of counts was expressed as the intensity of the pixel. Then the simulated image was compared with the observed image. The experimental conditions were as follows. A plastic fiber with a diameter of 0.5 mm was scanned with a nuclear plate, applying 30 keV monochrome X-rays at BL-14C in PF-KEK.

Results

The profile of the refraction contrast image is shown in Fig. 3 (single 100 [μm] cylinder), and the calculated images of the two columns are shown in Fig. 4A-1. It can be observed that pairs of bright and dark lines are produced in the boundary area, and the brightest/darkest spots come from overlap of bright/dark lines (magnified in Fig. 4B). The observed image of crossed glass fiber (500 μm) using an analyzer crystal at 30 keV is shown in Fig. 5. The distance between the nearest fiber and detector was 1.0 mm. The distance between two fibers was 2.0 mm. A simulated image of crossed fibers obtained using an analyzer crystal is shown in Fig. 6. The two images show good coincidence. The profile curves of observed and simulated images of two crossed fibers are shown in Fig. 7.

Discussion

X-ray beams apparently refract at the boundary of objects. The contrast between the bright line produced at the low specific gravity side (air) and the dark line at the high specific gravity side (blood vessels) is much

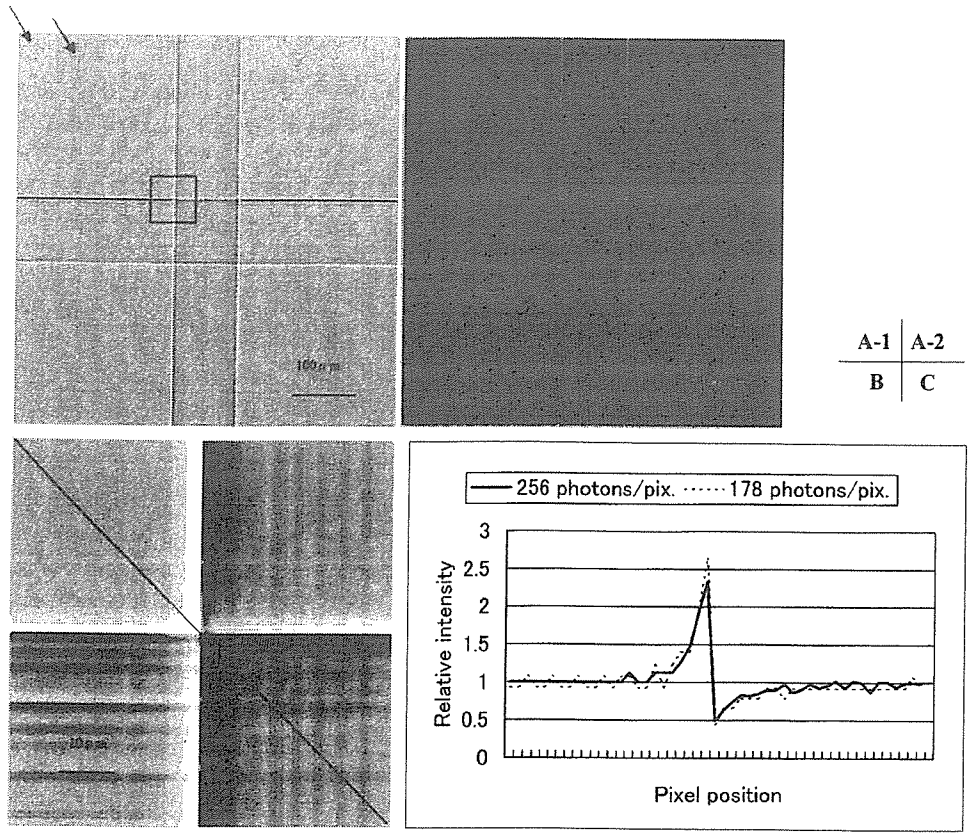

Fig. 4
A-1: Refraction image (256 photons/pix.) of two crossed 100 μm cylinders. *Arrows* show artifact pattern (vertical and horizontal lines) due to discontinuity.
A-2: Refraction image (178 photons/pix.) of two 100 μm cylinders.
B: Magnified image of the rectangular area in Fig. 4A.
C: Solid diagonal line profile of Fig. 4B.

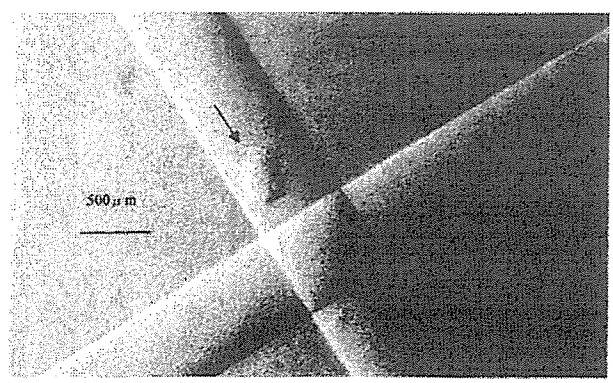

Fig. 5. Image of crossed glass fibers (500 μm) using analyzer crystal at 30 keV. *Arrow* shows debris.

larger than that of absorption. The overlap of the above-mentioned contrast generates the contrast-enhanced border spots due to the additional enlargement of contrast.

Under the condition of this simulation, the contrast of the brightest spot compared with the darkest spot that was produced by the overlapping of two fibers was 1.6 times larger than the contrast of the light-and-dark line at the margin of the obstacle (Figs. 3, 4C), and has the potential to be clearly useful for diagnostic ability. However, there is a possibility of interfering with diagnosis. Many bright and dark spots are produced in the

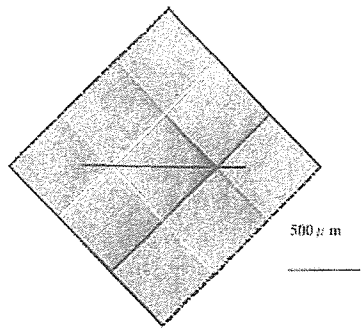

Fig. 6. Simulated image of crossed fibers obtained using an analyzer crystal. The two images show good coincidence at 30 keV.

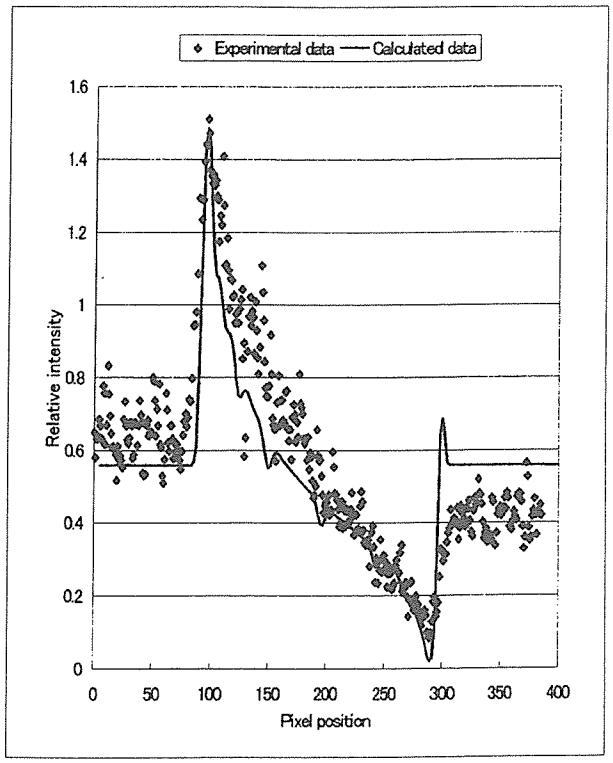

Fig. 7. Profile curves of observed and simulated images (solid line profile of Fig. 6).

case of many overlapping vessels. Further, small ringing artifact is observed in Fig. 4C due to discontinuity of the calculation. The artifact is regarded as digital noise that results from digitizing photon counts at each pixel of the detector. A simulated image is shown in Fig. 4A-1. Photon numbers are 256 at one pixel in Fig. 4A-1. A simulated image is shown in Fig. 4A-2, and photon numbers are 178 in this image. A profile curve is shown in Fig. 4C. For the same reason, the horizontal column in Fig. 4A-1 has the artifact pattern at the boundary area. For example, the ratio of vertical line intensity shown by the arrow to background intensity is 1.0625 in Fig. 4A-1.

Although the interference caused by the overlap of objects can be simulated with the Maxwell equation, the calculation performed in this study may be a good calculation method as a primary approximation of the Maxwell equation.[4] Simulation of and experimentation on X-ray absorption and interference by multiple-objects have just started, and more study is needed. The ray tracing method is useful as calculation tool for the above-mentioned simulation, and we will continue further research.

REFERENCES

1) Snigirev A, Snigireva I, Kohn V, *et al.* On the possibilities of x-ray phase contrast micro-imaging by coherent high-energy synchrotron radiation. *Rev Sci Instrum*, 66: 5486–5492, 1995.
2) Yagi N, Suzuki Y, Umetani K, Kohmura Y, Yamasaki K. Refraction-enhanced x-ray imaging of mouse lung using synchrotron radiation source. *Med Phys*, 26: 2190–2193, 1999.
3) Yamasaki K, Hirano M, Nagai H, *et al.* Refraction-enhanced X-ray imaging using synchrotron radiation source. *TECHNICAL REPORT OF IEICE*, MI2001–46: 15–20, 2001.
4) Stam J, Languenou E. Ray tracing in non-constant media. In *7th EUROGRAPHICS Workshop on Rendering*, (Springer-Verlag), 1996.

Kobe J. Med. Sci., Vol. 52, No. , pp. , 2006

Impaired Response of Perforating Arteries to Hypercapnia in Chronic Hyperglycemia

XIMENA-SAYURI OIZUMI [1], TAICHI AKISAKI [1], YOSHIYUKI KOUTA [1], XIU Z. SONG [1], TOSHIHIRO TAKATA [1], TAKESHI KONDOH [2], KEIJI UMETANI [3], MASATSUGU HIRANO [3], KATSUHITO YAMASAKI [3], EIJI KOHMURA [2], KOICHI YOKONO [1] and TAKASHI SAKURAI [1]

[1] *Division of Internal and Geriatric Medicine, Kobe University Graduate School of Medicine*
[2] *Division of Neurosurgery, Kobe University Graduate School of Medicine*
[3] *Japan Synchrotron Radiation Research Institute, SPring-8, Sayo-gun, Hyogo, Japan*

Received 20 December 2005/ Accepted 20 January 2006

Key words: chronic hyperglycemia, hypercapnia, synchrotron radiation, cerebral vessels

Diabetes mellitus increases the risk of cerebrovascular disease, the effects of hypercapnia on CBF (cerebral blood flow) and cerebrovascular reactivity during diabetes are still inconsistent. Here, we have established a new microangiographic technique using synchrotron radiation (SPring-8, Japan), which enabled us to visualize rat cerebral vessels with high spatial resolution in real time. The goal of the study presented here was to identify the effects of chronic hyperglycemia on hypercapnia-induced vascular responses (endothelium-dependent vasodilatation) and nitric oxide (NO) donor- induced vascular responses (endothelium-independent) of perforating arteries and of the deeply located large cerebral arteries. We found a significant vasodilatation of rat perforating arteries after hypercapnia with a maximum diameter of approximately 140% of baseline in normal Wistar rats. Chronic hyperglycemia impaired vasodilatation of perforating arteries in genetically diabetic GK rats. SNP (sodium nitroprusside) caused a similar vasodilatation of perforating vessels in normal and chronic hyperglycemia, indicating that endothelium-dependent vasodilatation of perforating arteries may be specifically impaired in chronic hyperglycemia. Possible impairment of endothelium-dependent vasodilatation in perforating vessels during chronic hyperglycemia may cause decreased vascular reserve capacity of perforating artery, resulting in the increased ischemic insults and cerebrovascular diseases in diabetes.

Diabetes mellitus involves long-term vascular complications and hyperglycemia is recognized as the main cause in the pathogenesis of these diabetic vasculopathies. In brain, diabetes increases the risks of large and small cerebrovascular diseases and makes patients demonstrably more susceptible to cerebral ischemia (1). Hyperglycemia has been shown to increase neurologic deficits in models of hypoxic-ischemic-injury and it is possible that differences in the regulation of cerebral blood flow (CBF) could be responsible for this susceptibility (2).

Hypercapnia is a potent dilator of cerebral blood vessels, but the effects of hypercapnia on CBF and cerebrovascular reactivity during diabetes are still inconsistent. In human studies, impaired vascular responses to hypercapnia have been reported (3-5), while in animal

Phone: + 81-78-382-5901 Fax: + 81-78-382-5919 E-mail: sakurai@med.kobe-u.ac.jp

experiments it has been found that CBF responses to hypercapnia of cortical arterioles are comparable to normal animals (6-10).

Perforating arteries are terminal vessels directly emerging from the main cerebral arteries and particularly important because these arteries supply blood to brain structures such as basal ganglia, thalamus and hippocampus that are frequently impaired in diabetes (11). Distinctive branching pattern and higher intraluminal pressure of perforating artery may suggest the differential regulation of vascular reactivity from that of the pial arterioles. However, to our knowledge, there is not any report about the vascular response of perforating arteries in vivo. In this study, we used a newly developed microangiographic technique and investigated the vascular response to hypercapnia of rat perforating arteries. Therefore, the goal of the study presented here is to identify the effects of chronic hyperglycemia on hypercapnia-induced vascular responses (endothelium-dependent vasodilatation) and nitric oxide (NO) donor-induced vascular responses (endothelium-independent) of perforating arteries and of the deeply located large cerebral arteries.

METHODS

Experimental design and animal preparation

All experimental procedures were performed following the guidelines for animal experimentation at Kobe University Graduate School of Medicine. Six month-old Male Wistar-Kyoto and Goto-Kakizaki (GK) rats weighing 400 g - 450 g and 300 g - 350 g, respectively, were used. Animal rooms were controlled for temperature (23℃), humidity (55%) and light (12 h light-dark cycles).

In order to investigate the effects of hypercapnia on cerebral vascular reactivity, we divided the experimental animals into two groups. The first group compromised control Wistar rats (n=13). The second group compromised genetically diabetic GK rats (CLEA, Tokyo, Japan) (n=10). For the hypercapnic challenge rats inhaled CO_2 at 12% mixed in air for 5 min. Then rats were allowed to a 15 min period of recovery under normal capnia. To investigate the endothelium-independent vascular vasodilatation we applied sodium nitroprusside (SNP) (0.5 μg.kg -1.min-1, i.v.).

Microangiography and image analysis

Microangiographic imaging of the rat brain was performed at the third generation synchrotron radiation facility SPring-8 in Hyogo, Japan. The experimental arrangement for X-ray imaging using monochromatic synchrotron radiation X-rays at the SPring-8 BL20B2 beamline has been fully described elsewhere (12, 13) (Fig. 1). In brief, we used monochromatic synchrotron radiation as an X-ray source, which was obtained from an 8 GeV electron storage ring (Beamline BL20B2, SPring-8, Hyogo, Japan). X-Ray was monochromatized at 17 keV energy using a silicon double-crystal monochromator. The camera head incorporates an X-ray direct-sensing pick-up tube (Saticon). Absorbed X-rays in the photoconductive layer of the tube are directly converted into electron-hole pairs, and signal charges are read out by electron beam scanning. The digital images were acquired as 1024×1024 pixels with 10-bit resolution after analog-to-digital conversion. The field of view was 9.5 × 9.5 mm^2 and thus the pixel size was approximately 9.5 μm.

Under anesthesia (pentobarbital sodium, 50 mg/kg i.p.), rats were placed in the supine position in a stereotaxic frame with a window of 3 cm × 4 cm in the center of the platform for direct radiation of the head. After tracheotomy, each animal received pancuronium bromide (0.8 μmol/kg) and was mechanically ventilated with room air using a ventilator (SAR 830/P ventilator, California, U.S.A.) at a rate of 60-70 respirations/min. One femoral

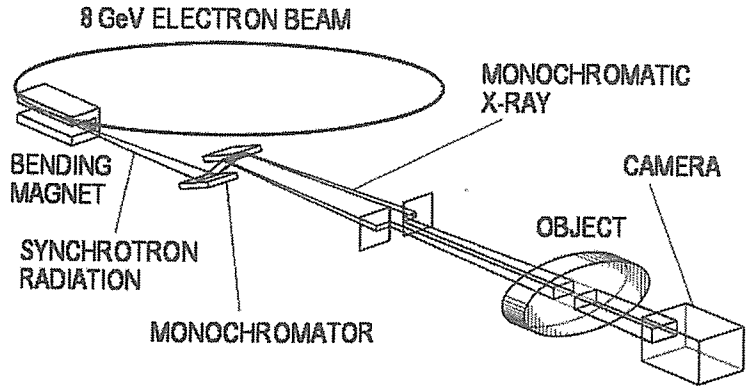

Figure 1 Illustration of the experimental arrangement at **BL20B2** beamline.

artery and one femoral vein were cannulated with PE-50 tubing (Natsume Manufacturing, Tokyo, Japan). The artery line was to measure systemic arterial blood pressure using a disposable pressure monitoring kit (Life Kit, Nihon Kohden, Tokyo, Japan) connected to a computer (Unique Acquisition, Unique Medical Company, Osaka, Japan). A femoral vein catheter was implanted for drug administration. Rectal temperature was maintained at 36-37℃ with a heating pad. The right external carotid artery (ECA) was cannulated. The PE-50 tube inserted was connected to an automated injector (Auto Injector 120S, Nihon Kohden, Tokyo, Japan) that was programmed to reproducibly deliver 0.2 ml of nonionic contrast media (Iomeprol, Daiichi Pharmaceutical Company, Tokyo, Japan) in 0.4 second for each microangiographic imaging. For consistent measurement of the vascular diameters of these arteries, we established an exact measuring point for each vessel. For the measurement of the internal carotid artery (ICA), we chose a point at a distance of 665 μm from the posterior communicating artery (Pcom), for the medial cerebral artery (MCA), a point at a distance of 475 μm distant from the ICA bifurcation. Because perforating arteries have many anatomical variations in number and origin of the vessels (14), we selected the largest branches emerging from the MCA and determined a measuring point at 190 - 380 μm distant from the MCA for each of the perforating arteries. Measurements of vessel diameters after repetitive angiography were made consistently at the same point. On the stored digital images, vessel diameters were measured semi automatically with a software (Image-Pro Plus ver.4.0, Media Cybernetics Inc., Silver Spring, MD, USA) combined with a program developed for this study (15).

Experimental protocol

The first angiogram was recorded to estimate the baseline diameter of the vessels. Hypercapnia was induced by inhalation of CO_2 at 12% mixed in air for 5min. The arterial blood gas were analyzed, and the inhalation was returned to normal room air. An additional angiograph was made at 15 min under normocapnia and arterial blood gases were analyzed. On separate experiments, an infusion pump was connected to the vein catheter and SNP was injected continuously at a flow rate of 0.4 ml/min

Measurements of blood gases and glucose

Arterial blood gas tensions and pH were measured with an i-STAT G3 + Cartridge (Abbott Point-of-Care, East Windsor, NJ, USA) and blood glucose concentrations were measured by a Glutest-S analyzer (Shiga, Japan).

Statistical analysis

Values are expressed as mean ± standard error. One way analysis of variance (ANOVA) was used for the comparison of more than two groups. Post-hoc comparisons between mean values were made with Scheffe's test. P value < 0.05 was accepted as statistically significant.

RESULTS

Table 1 shows the effects of CO_2 inhalation on the average pH, PaO_2, $PaCO_2$ of arterial blood gas from control and GK rats. We determined the initial diameter of each vessel before induction of hypercapnia, there was no statistical difference between the two groups. Baseline diameter for ICA was 232±17.8 μm and 278±45.2 μm, in Wistar and GK rats, respectively. For MCA, 211.4 μm±9.9 and 190.0±8.2 μm in Wistar and GK rats, respectively. For perforating arteries, baseline diameters were 77.1±4.6 μm and 91.5±9.8 μm in Wistar and GK rats, respectively. Figure 2 represents the response of perforating arteries to hypercapnia in control rats at baseline (Fig. 2A) and after 5 min of CO_2 administration (Fig. 2B).

Table 1. Arterial Blood Values

	WISTAR				GK			
	CO_2	O_2	pH	BS(mM)	CO_2	O_2	pH	BS(mM)
0 min.	30.9±4.1	107.1±5.6	7.5±0.1	6.5±0.5	33.3±2.7	101.8±6.5	7.4±0.1	15.2±1.4 *
5 min.	86.9±9.7	101.7±3.0	7.1±0.4	-	101.0±6.5	108.2±2.9	7.0±0.1	-
R15 min.	33.8±7.1	113.5±8.3	7.3±0.8	-	27.0±1.0	96±20.0	7.7±0.1	-

BS, blood sugar. 0 min, baseline. 5 min, after CO_2 administration. R15, room air.
Data are Mean±S.E. *P < 0.01 vs. control

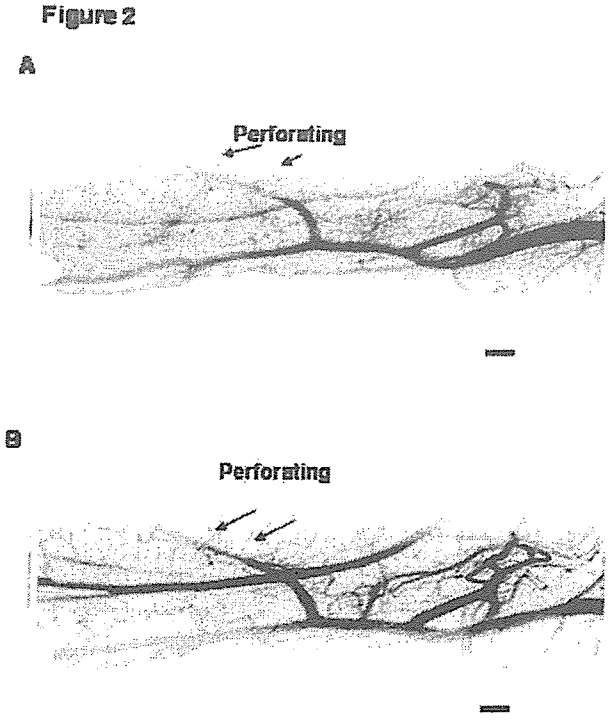

Figure 2
Photographs of perforating arteries emerging from the MCA (arrows) at rest (A), and during hypercapnia (B). Diameters of perforating vessels in this example were 80.5 μm at rest and 116.15 μm during hypercapnia respectively. Scale bar=300 μm.

Table 2 shows the steady-state responses to hypercapnia of the diameters in ICA, MCA and perforating vessels of normal Wistar and GK rats. In ICA and MCA we found a significant increase of diameter after 5 min hypercapnia for Wistar rat (126% and 142% of baseline diameter, respectively), GK rat also tended to show vasodilatation but failed to be significant. The vessel diameter returned to baseline value after the CO_2 challenge (Table 2). Perforating vessels showed significant vasodilatation to hypercapnia in the control group (135%), but in the GK group, vasodilatation was observed at insignificant rate (112%). The vessel diameter returned to baseline value after the CO_2 challenge (Table 2).

Table 2. Effect of hypercapnia on cerebral blood vessels

	Wistar			GK		
	ICA	MCA	PERF	ICA	MCA	PERF
0 min.	100	100	100	100	100	100
5 min.	126±6.8*	142±11.0*	135±11.3*	117±18.3	114±7.7	112±17.3
R15 min.	99±8.3	100±11	106±9.5	82±3.5	101±14.5	98±8.0

Values are means ± SE in % of change of baseline diameter.
5 min., CO2 inhalation. R15, room air 15 mins. *P < 0.01 from 0 min

Nitric Oxide donor, SNP, caused a significant vasodilatation of perforating arteries of both, control and GK groups (126% and 120%, respectively) (Table 3). ICA and MCA arteries did not show any significant changes (Table 3).

Table 3. Effect of SNP on cerebral blood vessels

	Wistar			GK		
	ICA	MCA	PERF	ICA	MCA	PERF
0 min.	100	100	100	100	100	100
10 min.	101±2.3	103±2.7	126±3.9**	105±4.0	110±3.0	120±7.8+

Values are means ± SE in % change of baseline diameter
10 min, 10 min. infusion of SNP. **P < 0.001 from 0 min. +P < 0.01 from 0 min.

DISCUSSION

This study is the first to directly investigate the effects of diabetes on the response of perforating arteries to hypercapnia and NO donor. We found a significant vasodilatation of rat perforating arteries with a maximum diameter of approximately 140% of baseline in normal Wistar rats after hypercapnia. In contrast, chronic hyperglycemia impaired vasodilatation of perforating arteries in genetically diabetic GK rats. Secondly, SNP caused a similar vasodilatation of perforating vessels in normal and diabetic rats, indicating that endothelium-dependent vasodilatation of perforating arteries may be specifically impaired in chronic hyperglycemia.

Previous experiments have reveled an intact CO_2 response of cerebral cortical arterioles in the diabetic dogs and STZ-induced diabetic rats (6, 8, 16). In contrast, human studies have (3-5) reveled that diabetic patients failed to respond normally to hypercapnia. Kadoi et al also suggested that the impaired response was related to severity of diabetes mellitus (5). The interpretation of clinical studies is complicated by the association of diabetes with microangiopathy and large vessel diseases. Therefore, we investigated the morphological changes in cerebral arteries in brains from 6-month and 12-month-old GK rats prior to this angiographic experiment. It has been reported that diabetes produces thickening of the

arterial wall, perivascular and interstitial fibrosis, microaneurysms, arteriolar hyalinosis, and atheromatosis (17-19), which could account for the pathogenesis of diabetic cerebrovascular disorders. In 6-month-old GK rats, however, cerebral arteries, including the MCA and perforating vessels did not show such microscopic alterations, nor could we find any significant microscopic changes in the of 12-month-old GK rats (data not shown). Thus, we think that the impaired reactivity to hypercapnia of deeply located vessels including perforating arteries could be due to hyperglycemia, rather than diabetic microangiopathy in GK brains.

In another set of experiments, we have analyzed the effects of hyperglycemia on the blood pressure induced vascular dilatation (autoregulation) of perforating arteries. We have found that autoregulatory responses were reversibly impaired in GK rats (data not shown), which supported the notion that perforating arteries of GK rats had functional loss of endothelium-dependent vasodilatation, rather than structural deficits of cerebral blood vessels. The discrepancy between previous findings and our findings may be related to the difference of animal models and/or the experimental technique such as anesthesia that could affect the vascular responses. Regional differences in the response of cerebral blood vessels have been specially noted in previous experiments (20).

Several mechanisms have been proposed for the hypercapnia induced cerebrovascular vasodilatation. Hypercapnia requires the development of extracellular acidosis (21-23). NO is a major mediator of endothelium-dependent relaxation in various vascular beds, and plays an essential role in regulation of the cerebral circulation. Iadecola et al. demonstrated that nitric oxide synthase (NOS) inhibitors attenuated the CBF response to hypercapnia that occurs only at $PaCO_2$ < 100 mmHg (24). You et al. suggested that the cerebral vasorelaxation elicited by CO_2 was not related with an increase in NOS activity (22). This might indicate that the cerebral vasodilatation elicited by hypercapnia has NO-dependent and NO-independent components. It is likely that NO plays a role in the response to hypercapnic acidosis and it is partly responsible for the increase of cerebral blood flow during hypercapnia (23, 25, 26). There is enough evidence of the existence of ATP-sensitive potassium channels (K_{ATP}) in cerebral blood vessels, and therefore their implication in the vasodilatation of cerebral arteries to hypercapnia has also been investigated. Faraci et al. found that glibenclamide attenuated the dilatation of cerebral arterioles in response to a low concentration of acetylcholine and moderate hypercapnia (27).

In diabetes, functional impairment of NO and K_{ATP} channels-mediated vasodilatation have been suggested of pial arterioles and the basilar artery (28-29). Diabetes is associated with an increased generation of oxygen-derived free radicals in vascular tissues, and reactive oxygen species could influence the structure and activity of K_{ATP} channels (19, 29-32). Continuous production of reactive oxygen species produces an impaired vascular response of perforating arteries during chronic hyperglycemia.

There is considerable controversy regarding the effects of NO donors on vascular reactivity. It has been reported that application of intracarotid SNP fails to augment CBF (33, 34), and that the degree of vasodilatation varies in iliac and superior mesenteric arteries (35). The discrepancy between experiments seems to be inconsistent across animal species and vascular bed examined. However, we could find that application of SNP increased the vascular diameter similarly in control and diabetic rats, suggesting that impaired vasodilatation of perforating arteries to hypercapnia is due to the deficit in NO production/release in vascular endothelium in part during chronic hyperglycemia.

In summary, we could demonstrate the in vivo evidences for the first time that responses of rat perforating arteries to hypercapnia are specifically disrupted during diabetes mellitus.

Possible impairment of endothelium-dependent vasodilatation in perforating vessels during chronic hyperglycemia may cause decreased vascular reserve capacity of perforating artery, resulting in the increased ischemic insults and cerebrovascular diseases in diabetes. Further studies are needed to know the cellular mechanism of hyperglycemic impacts on cerebrovascular reactivity.

ACKNOWLEDGEMENTS

We deeply appreciate Dr. Haruo Yamashita, Dr. Bo Yang, Dr. Yoshikazu Ryu, Dr. Takuya Teranishi, Dr. Abesh K. Bhattacharjee, Dr. Seiji Nakajima, Dr. Akitsugu Morishita, Dr. Masahiro Tamaki, Dr. Takashi Mizobe, Dr. Junji Koyama, Dr. Kazuhiro Tanaka and Dr. Keiji Kidoguchi for their technical assistance. This work was supported by a Research Grant from the Novartis Foundation for Gerontological Research and a Grant-in-Aid for Scientific Research (17500473) from Japan Society for the Promotion of Science (T.S.). Synchrotron radiation experiments were performed at the SPring-8 BL20B2 beamline with the approval of the Japan Synchrotron Radiation Research Institute (Acceptance Nos. 2002A0079-NL2-np, 2002B0312-NL2-np, and 2004A0313-NL3-np).

REFERENCES

1. **Karapanayiotides T, Piechowski-Jozwiak B, van Melle G, Bogousslavsky J, Devuyst G.** 2004. Stroke patterns, etiology, and prognosis in patients with diabetes mellitus. Neurology **11**; 62(9): 1558-62.
2. **LeBlanc MH, Huang M, Vig V, Patel D, Smith EE.** 1993. Glucose affects the severity of hypoxic-ischemic brain injury in newborn pigs. Stroke **24(7)**: 1055-62.
3. **Dandona P, James IM, Newbury PA, Woollard ML, Beckett AG.** 1978.Cerebral blood flow in diabetes mellitus: evidence of abnormal cerebrovascular reactivity. Br Med J. **2(6133)**: 325-6.
4. **Griffith DN, Saimbi S, Lewis C, Tolfree S, Betteridge DJ.** 1987.Abnormal cerebrovascular carbon dioxide reactivity in people with diabetes. Diabet Med., **4(3)**: 217-220.
5. **Kadoi Y, Hinohara H, Kunimoto F, Saito S, Ide M, Hiraoka H, Kawahara F, Goto F.** 2003. Diabetic patients have an impaired cerebral vasodilatory response to hypercapnia under propofol anesthesia. Stroke **34**: 2399-2403.
6. **Simpson RE, Phillis JW, Buchannan J.** 1990. A comparison of cerebral blood flow during basal, hypotensive, hypoxic and hypercapnic conditions between normal and streptozotocin diabetic rats. Brain Research, **531**: 136-142.
7. **Cenic A, Craen RA, Howard-Lech VL, Lee TY, Gelb AW.** 2000. Cerebral blood volume and blood flow at varying arterial carbon dioxide tension levels in rabbits during propofol anesthesia. Anesth Analg, **90**: 1376-1386..
8. **Sieber FE, Brown PR, Wu Y, Koehler RC, Traystman RJ.** 1993. Cerebral blood flow responsitivity to CO2 in anesthetized chronically diabetic dogs. Am J Physiol. **264**: H1069-H1075.
9. **Kawata R, Nakakimura K, Matsumoto M, Kawai K, Kunihiro M, Sakabe T.** 1998. Cerebrovascular CO2 reactivity during anesthesia in patients with diabetes mellitus and peripheral vascular disease. Anesthesiology **89(4)**: 887-893.
10. **Rodriguez G, Nobili F, Celestino MA, Francione S, Gulli G, Hassan K, Marenco S, Rosadini G, Cordera R.** 1993. Regional cerebral blood flow and cerebrovascular reactivity in IDDM. Diabetes Care **16(2)**: 462-468.

11. **Groot J, Leeuw FE, Oudkerk M, van Gijn J, Hofman A, Jolles J, Breteler M.** 2000. Cerebral white matter lesions and cognitive function: the Rotterdam Scan Study. Ann Neurol. **47**: 145-151.
12. **SPring-8.** 2000. Medical and Imaging I (BL20B2). SPring-8 Annual Report. **1999**: 54-55.
13. **Umetani K, Yamashita T, Maehara N, Tokiya R, Imai S, Kajihara Y.** 2003. Small-field angiographic imaging of tumor blood vessels in rabbit auricle using X-ray SATICON camera and synchrotron radiation. Proc. 25th Annual Int. Conf. of the IEEE Engineering in Medicine and Biology Society. Cancún 978-981.
14. **Rieke GK, Bowers DE, Penn P.** 1981. Vascular supply pattern to rat caudatoputamen and globus pallidus. Scanning electronmicroscopic study of vascular endocasts of stroke-prone vessels. Stroke **12**: 840-846.
15. **Hirano M, Yamasaki K, Sakurai T, Kondoh T, Ryu Y, Okada H, Sugimura K, Kitazawa S, Kitazawa R, Maeda S, Katafuchi T, Tamura S.** 2003. Measurement of blood vessel diameter for angiography using refraction contrast imaging. Igaku Butsuri: **23**:157-159.
16. **Wang Q, Pelligrino DA, Koenig HM, Albrecht RF.** 1994. The role of endothelium and nitric oxide in rat pial arteriolar dilatory responses to CO2 in vivo. J Cereb Blood Flow Metab,
17. **Muruganandan S, Srinivasan K, Gupta S, Gupta PK, Lal J.** 2005. Effect of mangiferin on hyperglycemia and atherogenicity in streptozotocin diabetic rats. J Ethnopharmacol **97(3)**:497-501.
18. **Velasquez MT, Kimmel PL, Michaelis OE 4th.** 1990. Animal models of spontaneous diabetic kidney disease. FASEB J. 4: 2850-2859.
19. **Yu Y, Ohmori K, Kondo I, Yao L, Noma T, Tsuji T, Mizushige K, Kohno M.** 2002. Correlation of functional and structural alterations of the coronary arterioles during development of type II diabetes mellitus in rats. Cardiovascular Research **56**: 303-311.
20. **Duckrow R, Beard D, Brennan R.** 1987. Regional cerebral blood flow decreases during chronic and acute hyperglycemia. Stroke **18**: 52-58.
21. **Kontos HA, Wei EP, Raper AJ, Patterson JL.** 1977. Local mechanism of CO2 action on cat pial arterioles. Stroke **8**:226-229.
22. **You JP, Wang Q, Zhang W, Jansen-Olesen I, Paulson OB, Lassen NA, Edvinsson L.** 1994. Hypercapnic vasodilatation in isolated rat basilar arteries is exerted via low pH and does not involve nitric oxide synthase stimulation or cyclic GMP production. Acta Physiol Scand **152**: 391-397.
23. **Tian R, Vogel P, Lassen NA, Mulvany MJ, Andreasen F, Aalkjaer C.** 1995. Role of extracellular and intracellular acidosis for hypercapnia-induced inhibition of tension of isolated rat cerebral arterioles. Circ Res **76**: 269-275.
24. **Iadecola C, Zhang F.** 1994. Nitric oxide-dependent and –independent components of cerebrovasodilatation elicited by hypercapnia. Am. J. Physiol. **266**: R546-R552
25. **Iadecola C.** 1992. Does nitric oxide mediate the increases in cerebral blood flow elicited by hypercapnia?. Proc. Natl. Acad. Sci. **89**: 3913-3916.
26. **Wang Q, Palson OB, Lassen NA.** 1992. Effect of nitric oxide blockade by NG-nitro-L-arginine on cerebral blood flow response to changes in carbon dioxide tension. J. Cereb. Blood Flow Metab. **12**: 935-946.
27. **Faraci FM, Breese KR, Heistad DD.** 1994. Cerebral vasodilatation during hypercapnia. Role of glibenclamide-sensitive potassium channels and nitric oxide. 1994. Stroke **25**: 1679-1683.

28. **Mayhan W, Faraci F.** 1993. Responses of cerebral arterioles in diabetic rats to activation of ATP-sensitive potassium channels. Am. J. Physiol. (Heart Circ. Physiol. **34**): H152-157.
29. **Matsumoto T, Yoshiyama S, Wakabayashi K, Kobayashi T, Kamata K.** 2004. Effect of chronic insulin on cromakalim-induced relaxation in established streptozotocin-diabetic rat basilar artery. Eur. J. Pharmac. **504**: 129-137
30. **Faraci FM, Heistad DD.** 1998. Regulation of the cerebral circulation: role of endothelium and potassium channels. Physiol Rev. **78**: 53-97.
31. **Niedowicz DM, Daleke DL.** 2005.The role of oxidative stress in diabetic complications. Cell Biochem Biophys. **43**: 289-330.
32. **Erdos B, Simandle SA, Snipes JA, Miller AW, Busija DW.** 2004. Potassium channel dysfunction in cerebral arteries of insulin-resistant rats is mediated by reactive oxygen species. Stroke **35**: 964-9.
33. **Young WL, Prohovnik I, Schroeder T.** 1990. Intraoperative 133Xe cerebral blood flow measurements by intravenous versus intracarotid methods. Anesthesiology **73**: 637-643.
34. **Joshi S, Duong H, Mangla S, Wang M, Libow AD, Popilskis S, Ostapkovich ND, Wang TS, Young WL, Pile-Spellman J.** 2002. In nonhuman primates intrcarotid adenosine, but not sodium nitroprusside, increases cerebral blood flow. Anesth Analg **94**: 393-399.
35. **Martinez-Nieves B, Dunbar JC.** 1999. Vascular dilatatory responses to sodium nitroprusside (SNP) and α-adrenergic antagonism in female and male normal and diabetic rats. P.S.E.B.M. **222**: 90-98.

Title: Neuroprotective Effect of D-Fructose-1,6-Bisphosphate Against β-Amyloid Induced Neurotoxicity in Rat Hippocampal Organotypic Slice Culture: Involvement of PLC and MEK/ERK Signaling Pathways.

Authors: XiuZhen Song [a], Bin Wu [b], Toshihiro Takata [a], XiaoNan Wang [a], XimenaSayuri Oizumi [a], Taichi Akisaki [a], Koichi Yokono [a] and Takashi Sakurai [a] *,

a :Department of Internal and Geriatric Medicine,
Kobe University Graduate School of Medicine,
7-5-1 Kusunoki-cho, Chuo-ku, Kobe 650-0017, Japan
b : Open Research Center of Lifestyle-Related diseases
Mukogawa-Women's University
6-46 Ikebiraki-chome, Nishinomiya 663-8558,Japan
* Corresponding author: Takashi Sakurai
E-mail: sakurai@med.kobe-u.ac.jp
Tel: +81-78-382-5901
Fax: +81-78-382-5919

Total number of pages: 28
Figures: 6
Abstract words: 225

1. Introduction

Alzheimer's disease (AD) is a progressive senile dementia characterized by deposition of amyloid β-peptide (Aβ) in the form of senile plaques and the microtubule associated protein tau as paired helical filaments. Aβ is a 4 kDa peptide of 39-42 residues which has multi neurotoxic effects leading to the dysfunction and death of neurons(Yanagisawa,2000). Both in vitro and in vivo studies have confirmed the crucial role of Aβ in the development of AD. Progressive neuronal loss in AD is considered to be a consequence of the neurotoxic properties of Aβ (Iwata et al.,2005). From this point of view, preventing the Aβ-induced neurotoxicity is of great important for the development of potent therapeutic strategies.

D-fructose-1,6-bisphosphate (FBP), an endogenous intermediate of glycolytic pathway, can protect organ system from lethal injury accompanying ischemia or shock (Markov et al.,1983). There is some other evidence that FBP attenuates brain damage induced by hypoxia-ischemia (Izumi et al.,2003), insulin induced hypoglycemia (Fairas et al., 1986) and cardiogenic shock (Zhang et al.,1988). FBP is also reported provide protection of neurons against simulated ischemia in hippocampal slices (Liniger et al., 2001). The mechanisms by which FBP protects the brain neurons are not well understood. Possible mechanisms of protection include anaerobic metabolism of FBP to yield ATP (Gobbel et al.,1994) or it's ability to reduce ATP loss (Gregory et al, 1990), calcium chelation (Hassinen et al.,1991) and modulation of second messenger system.

Up to date, whether the neurotoxicity of Aβ in hippocampus could be antagonized by FBP is not well documented. We conducted this study to examine if FBP has the neuroprotective effect against Aβ-induced toxicity using organic hippocampal slices. Furthermore, to determine whether FBP serves as an alternative energy sources to preserve neuronal survival, we examined the effects of exogenous FBP on ATP levels in organic hippocampal slices during Aβ neurotoxication. Recently many studies also indicate that FBP exerts its neuroprotective effect by modulating intracellular signaling pathways. A few intracellular signaling pathways, such as PLC and MEK/ERK (Fahlman et al., 2002) are reported to be associated with the neuroprotective effects of FBP, and thus we investigated here if these pathways involved in the effects of FBP on the Aβ-induced neurotoxicity.

2 Materials and methods

The experiments were conducted according to the guideline of animal experimentation at the Kobe University School of Medicine and conform to relevant National Institution of Health guidelines.

2.1 Preparation of organotypic hippocampal slices

Hippocampal slices were made from the septal half of the hippocampus using a standard method (Sakaguchi et al., 1994). Briefly, 9-11 days Wistar rats (Hartley, SLC, Japan) were anesthetized with 98% Diethyl Ether and decapitated. The hippocampi were rapidly dissected at 4-6℃ and cut into 450μm slices using a Mcillwain Tissue Chopper (Mickle Laboratory Engineering Co.Ltd, UK). Slices were then transferred

onto 30-μm diameter-pored membrane （Millicell-CM, Millipore, Bedford, MA, USA）, and put into a six-well microplate (Costar Corning Inc, NY,USA) with 1ml slice culture media per well. The culture media were contain 50% Eagles minimal essential medium (MEM) (Gibco,CA,USA), 25% Hanks' Balanced Salt Solution (HBSS) (Gibco,CA,USA), 25% heat inactivated horse serum (Gibco,CA,USA) containing 1% penicillin/streptomycin. Slices were kept in culture for 14 days before study and the six-well micropaltes were stored at 37℃ in a 95% humidified atmosphere with 5% CO_2 incubator (Sanyo, Tokyo, Japan) untill use.

2.2 Treatment of hippocampal slices

Slices in six-well micropaltes at day 14 were washed, and the basic medium was replaced with various agents for the treatment. The basic medium contained 90mM NaCl, 4mM KCl, 0.1mM $MgCl_2$, 0.1mM KH_2PO_4 , 0.5 mM $MgSO_4$, 0.1 mM Na_2HPO_4, 0.5 mM NaH_2PO_4, 14 mM $NaHCO_3$, 1.2 mM $CaCl_2$, 10 mM glucose, about 2 mM essential and non-essential amino acids, 0.02 mM vitamins. To establish the Aβ-induced neurotoxicity, slices were treated with three kinds of Aβ pepetides ($A\beta_{25\text{-}35}$, $A\beta_{1\text{-}40}$, and $A\beta_{1\text{-}42}$) in various concentrations. $A\beta_{25\text{-}35}$, $A\beta_{1\text{-}40}$, and $A\beta_{1\text{-}42}$ (Peptide Institute Inc. Japan, Osaka) were dissolved in sterilized distill water. To assure full contact between Aβ and the culture, treatment media was applied from underneath the insert onto the culture by pipetting at first 4h. Various concentrations of FBP (Sigma, St.Louis, MO,USA) were added to the culture with or without $A\beta_{25\text{-}35}$ for determining the FBP's effect against the Aβ induced neurotoxicity. To determine whether a signaling pathway is involved in the neruoprotective effect of FBP, a few signaling pathway-specific inhibitors were used, including a phospholipase-C (PLC) inhibitor, U0126 (Wako, Osaka, Japan), a mitogen activated extracellular signal protein kinase (MEK1/2) inhibitor, U-73122 (Wako, Osaka, Japan), an extracellular signal activated protein kinase (ERK) inhibitor, PD98059 (Wako, Osaka, Japan), and a protein kinaseC (PKC) inhibitor, chelerythrine (Calbiochem Merck,Tokyo, Japan). Each pathway-specific inhibitors (10 μM) was added into the slice culture with or without various concentrations of FBP and $A\beta_{25\text{-}35}$.

2.3 Assessment of cell death in hippocampal slices

Propidium iodide (PI) method was applied for the assessment of neuron death in hippocampal slices at 24h, 48h, and 72h after each treatment in the CA1 region of the hippocampus. To label the nuclei of dead neurons, 4.6μg /ml PI (Sigma, Louis.St, Mo,USA) was added to the wells of the culture microplates for 15 min. After 15 min, digital imagines of PI fluorescence were obtained with an inverted fluorescence microscope equipped with a digital camera (Olympus IX70, Tokyo, Japan). After the final image, all the neurons were killed by adding 10 μM N-Methyl-D-Aspartic Acid （NMDA） and the final PI fluorescence intensity was adjusted equivalent to 100% cell death. The mean intensity (green values) of the PI fluorescence were measured using an image program MacScope (Ver 2.6.1, Mitani Inc, Osaka, Japan).

2.4 Measurement of ATP levels.

Hippocampal slices were dissected under a microscope at 48h after each treatment. Four slices were immediately homogenized in 0.5 N perchloric acid with 1 mM thylenediaminetetra acetic acid and centrifuged for 15min at 2000rpm. The

supernatant was neutralized with 2M $KHCO_3$, recentrifuged and stored at -30℃ until assay of ATP. ATP was quantitated enzymatically and fluorometrically by measuring the production of nicotinamide adenine dinucleotide phosphate hydride (Sakurai et al., 2002). Protein content of the slices was determined by the method of Lowry and Passonneau (Okada et al.,1974).

2.5 Statistical analysis

Date was expressed as mean ± standard error of the mean (s.e.m) from three independent experiments. Statistical significance was established by ANOVA followed by post-hoc test using SPSS (Ver 12.0, SPSS. Inc., Chicago, USA) software. $P<0.05$ was considered to be statistically significant.

3. Results

3.1 Neurotoxicity of Aβ

Three different kinds of Aβ fragments, $A\beta_{25-35}$, $A\beta_{1-40}$, and $A\beta_{1-42}$, were applied to establish the neurotoxicity of Aβ. Cell death was evaluated at 48h after various concentrations of three Aβ fragments administration. $A\beta_{1-40}$, and $A\beta_{1-42}$ caused up to 40%-70% cell death at concentrations ranging from 0.5 μM-50 μM. $A\beta_{25-35}$ (50 μM) induced similar toxicity comparable to $A\beta_{1-40}$, and $A\beta_{1-42}$ at 25 μM (data not shown). Since $A\beta_{25-35}$ and full length $A\beta_{1-42}$ cause neuron death by similar mechanisms (Mattson, 1997), $A\beta_{25-35}$ 50 μM was used in all subsequent experiments.

3.2 Neuroprotective effect of FBP in hippocampal slices

Various concentration of FBP (0 mM, 1.7 mM, 3.5 mM, 7 mM, 10 mM) were added to the media. Compared with control group (FBP 0 mM), the addition of FBP significantly reduced the cell death in hippocampal slices at 24h, 48h and 72h after treatment (shown in Fig. 1). Interestingly, this neuroprotective effect of FBP was not in a dose-dependent manner. Compared with other FBP concentration groups, FBP 3.5 mM has better neuroprotective effect than those of other FBP groups (FBP 3.5 mM group *vs* other FBP concentration groups, all the $P<0.01$).

3.3 Neuroprotective effect of FBP against Aβ induced neurotoxicity in hippocampal slices.

As shown in Fig.2, treatment with FBP significantly decreased Aβ induced cell death in hippocampal slices at 24h, 48h and 72h (All the FBP concentration groups compare with control group, $P<0.01$). Similarly, this neuroprotective effect of FBP against Aβ was not in a dose-dependent manner. FBP 3.5 mM group has better neuroprotective effect than that of other FBP concentration groups (FBP 3.5mM+Aβ group *vs* other FBP concentration groups, all the $P<0.01$)

3.4 Neuroprotective effect of FBP against Aβ induced neurotoxicity was attenuated by PLC, MEK or ERK inhibitors

Some other studies suggested that the neuroprotection action of FBP against hypoxia was dependent on PLC, MEK/ERK pathways, and this was also found to be the case with the hippocampal slices when exposure to Aβ induced neurotoxicity. Protective effect of FBP 3.5 mM against Aβ induced neurotoxicity in hippocampal slices was abolished by PLC inhibitor, U73122, MEK inhibitor, U0126, and ERK inhibitor, PD98059 at 24h, 48h and 72h. However, administration of chelerythrine, a protein kinase C inhibitor, did not modulate the neuroprotection of FBP against Aβ

induced neurotoxicity in hippocampal slices (Fig. 3).

3.5 Effects of FBP on the ATP levels of hippocampal slices in the presence or absence of Aβ.

To test the hypothesis whether the neuroprotective action of FBP against Aβ induced neurotoxicity was due to its role as an alternative energy source, we examined the effect of various concentrations of FBP on the ATP levels in hippocampal slices in the presence or absence of Aβ. Compared with control group (FBP 0mM), FBP groups (concentration raging from 1.7 mM to 10 mM) had significant elevated ATP levels in hippocampal slices at 24h and 48h in the absence of Aβ (all the $P<0.001$) . The ATP levels were not significantly different among these FBP groups (Fig.4). With the presence of Aβ, the results were similar with those without Aβ, and the ATP levels were preserved at each concentration of FBP (compare with FBP 0 mM+Aβ group, all the $P<0.001$) . However, the difference of the ATP levels among these various FBP concentration groups did not reach to significance (Fig. 5).

3.6 Effects of PLC, MEK, ERK or PKC inhibitors on the ATP levels in hippocampal slices in the presence of FBP and Aβ.

To investigate whether energy metabolism is involved in the neuroprotective action of FBP against Aβ toxicity through specific signaling pathways, ATP levels were examined when co-treated with specific inhibitors. Compared with control group (FBP 3.5 mM+ Aβ), the addition of PLC inhibitor, MEK inhibitor, ERK inhibitor or PKC inhibitor did not cause significant difference in the ATP levels in hippocampal slices at 24h and 48h (Fig.6).

4. Discussion

We have shown that exogenous FBP reduced Aβ induced cell toxicity in rat hippocampal slices. This neuroprotective effect of FBP might be the result of additional supply of ATP in the hippocampal slices. However, the neuroprotective action of FBP against Aβ induced neurotoxicity was not in a dose-dependent manner, and the ability of FBP to produce or preserve ATP was also not in a dose-dependent manner. The results therefore suggested that protective action of FBP against Aβ induced neurotoxicity in hippocampal slices was due to, at least in part, other than its role as an alternative energy substrate to yield additional ATP. Furthermore, co-treatment of specific signaling pathways inhibitors with FBP and Aβ redueced the cell viability without alternating of ATP levels, suggesting that protective action of FBP against Aβ induced neurotoxicity was not only due to the alternative energy source, but also a modulator for neuroprotective signaling pathways.

FBP has been shown to attenuate tissue damage resulted from myocardial or kidney ischemia (Fairas et al.,1986; Didlake et al.,1989). Many studies demonstrated that FBP has neuroprotective effect in central nervous system against hypoxia/ischemia (Sola et al.,1996; Takata et al.,1997). Here we showed that FBP attenuated the neuron death induced by Aβ in hippocampal slices in a non dose-dependent manner, and also the ability of FBP to preserve the ATP levels appeared not related to its concentrations. Because of its role as an intermediate products in glycolysis, it has been widely assumed that the protective effects of exogenous FBP are resulted from

its serving as an additional substrate for glycolysis (Hardin and Roberts ,1994). But our findings didn't seem to consist with this hypothesis since the increasing of FBP could not lead to the ATP elevation in a dose-dependent manner in hippocampal slices during Aβ exposure. To our knowledge, there are no specific transporters for FBP in the central nervous system. FBP is a highly negative charged molecular which is not easy to across the hippocampal cellular membranes. Considering the fact that FBP was not taken up by red blood cell (Rigobello et al., 1982) or myocardial tissue (Galzigna et al.,1989), it was hypothesized the FBP would first have to undergo hydrolysis to fructose in order to be utilized. However some other experiments have demonstrated that, unlike FBP, addition of fructose or fructose-6-phosphate did not have neuroprotective effects (Gregory et al., 1989). It seems that relatively small amounts of exogenous FBP could be metabolized by hippocampal slices.

While it seems only small amount of FBP could be uptaken by hippocampal culture cells, and they are probably insufficient to explain its role as an energy substrate to maintain ATP level in hippocampal slice cultures. However, we could not exclude the possibility that this level of FBP might be sufficient to regulate energy metabolism and to modulate intracellular second messenger system. Some investigators illustrated that exogenous FBP has biphasic effects on the neuronal cellular metabolism. On one hand, FBP promotes glucose metabolism in astrocytes via pentose phosphate pathway (PPP; Kelleher et al.,1995). PPP is quite active in the CNS (Zubairu et al.,1983; Larrabee 1980) and stimulation of PPP may lead to the increasing production of NADPH, synthesis of fatty acids, triglycerides, and phospholipids, then reduces oxygen radical injury of neural cell by regulating glutamine peroxidase (Lazzarino et al.,1987; Tavazzi et al.,1990). On the other hand, exogenous FBP may reduce the uptake of glucose from extracellular environment (Kelleher et al.,1995), and, moreover, it could inhibit the activity of phosphorfructokinase (PFK)-the key enzyme of glycolysis, therefore reduce the production of lactate and the activity of TCA cycle (Kelleher et al.,1995). Our findings that neither higher nor lower levels of FBP cause better neuroprotective effects could be partially explained by this dual effects of FBP on the metabolism of neural cells.

Besides its role for serving as a metabolism regulator in the neruoprotective effects of FBP, the possible involvement of FBP in several intracellular signaling pathways should be taken into account. Recent studies have shown that neuroprotective qualities of FBP on hypoxia/ischemia- induced toxicity in hippocampal slices are dependent on PLC (Donohoe et al.,2001) and MEK/ERK pathways (Fahlman et al.,2002). In consistent with these studies, our observations also imply that PLC and ERK/MEK pathways are involved in the neuroprotective effects of FBP against Aβ induced neurotoxicity in hippocampal slices. Co-administration of PLC or ERK/MEK pathway inhibitors attenuate the neuroprotective action of FBP, but without affecting the ATP levels in hippocampal slices. Intracellular signaling pathways play crucial roles in regulating the cellular response and survival following insults by neurotoxins such as Aβ. Since little of exogenous FBP could enter neurons to serve as a signal, it was hypothesized that FBP might initiate its neuroprotective signaling at or near the cell surface. On the cell surface, FBP stimulate lipolysis

(Chlouverakis,1968) through PLC pathway and increase the production of diacylglycerol and inositol triphophate, leading to the elevation of intracellular Ca^{2+}. The consequence of this event is the activation of MEK/ERK signaling pathway and the expression of neuroprotective genes. Another important intracellular signaling system is PKC, a family of 12 serine/threonine kinase (Musashi et al., 2000). Since PKC has been found to modulate cell vialibility resulting in the protection of various neuronal cells (Saito and Shirai, 2002), we also investigated here if PKC pathway was involved in the neuroprotection of FBP. However our data indicate that co-treatment of PKC inhibitor did not make significant alternations of both cell death and ATP levels in hippocampal slices in the presence of FBP and Aβ, suggesting that PKC signaling pathway may not be involved in the neuroprotective effects of FBP against Aβ induced neurotoxicity in hippocampal slices.

In the present study, we first report that FBP has neuroprotective effects against Aβ induced neurotoxicity in hippocampal slices. The preservation of ATP and the involvement of PLC and MEK/ERK signaling pathways could explain FBP's role as a modulator for both energy metabolism and intracellular signaling pathways. Even more, some recent studies have revealed that FBP has immunomodulatory (Bordignon et al.,2003) and anti-inflammatory properties (Alves et al.,2004; Nunes et al., 2003) in modulating cellular function. The mechanism of FBP's neuroprotective effects seems to be multifactorial, and extensive studies are required to reveal its complex roles as a neuroprotectant.

Acknowledgements

This work was supported by a Research Grant from the Novartis Foundation for Gerontological Research and a Grant-in-Aid for Scientific Research (17500473) from Japan Society for the Promotion of Science. We deeply appreciate Dr. Sakaguchi, T., and Dr. Yang., B for technical assistance.